Dose requirements in stereoradiography

Predrag R. Bakic, Michael Albert, and Andrew D. A. Maidment
Thomas Jefferson University, Philadelphia, PA 19107

ABSTRACT

Stereoscopic viewing of radiographic images is advantageous in reducing ambiguity due to background anatomic noise. This advantage is usually considered to be balanced by doubling the dose required for acquisition of a stereo image pair. In the case of a quantum-noise limited detector, detection theory suggests a possible decrease of the dose by half. We tested this assumption by a series of contrast-detail observer experiments, using phantom images acquired over a range of exposures. The number of visible details, the effective reduction of the dose, and the effective decrease in the threshold SNR were compared for the acquired images viewed mono- and stereoscopically. Experimental results support our hypothesis for the images acquired at lower exposures. The quantum noise is more evident in the lower exposure images, corresponding to the quantum noise limited detection case. With increasing exposure, the observed dose benefit of stereoradiography decreased, but was always positive. Potential reasons for the reduced benefit observed with higher exposures are discussed.

Keywords: Digital radiography, stereoradiographic technique, dose, observer study, human perception.

1. INTRODUCTION

A significant limitation of projection radiography is that relevant findings are often obscured by the x-ray shadows of other anatomical structures, while non-existent pathologies can be mimicked by such effects (summation artifacts). The advantage of stereoradiographic techniques in handling such issues is mentioned in several radiographic text books and articles, but issues of dose are either not mentioned[1–3] or it is suggested that a stereographic technique requires a total of twice the exposure of a single-projection technique.[4] In situations where the dose is set by the limitations of quantum mottle (as opposed to the H-and-D curve of the film or other detector limitations) signal detection theory suggests that an ideal observer would be able to combine information from the two stereoscopic views and thereby suppress quantum mottle. Thus, under this model, two stereoscopic views, each acquired with one half of the dose of a single-projection radiograph, would provide the same level of resilience to quantum noise, but give the inherent benefits of stereoscopic viewing.

The psychophysical literature documents that for many visual tasks the use of two eyes is more efficacious than the use of one.[5,6] In particular, threshold measurements of sinusoidal patterns have shown a decrease in threshold (i.e., an increase in sensitivity) of a factor of $\sqrt{2}$ when viewing is performed binocularly as opposed to monocularly,[7] precisely as expected for an ideal observer combining the signal from each eye. The quantum mottle in x-ray projections is different from the sources of noise in these experiments, however, in that at the time of acquisition a given realization of the noise is permanently recorded and thus is presented to each eye as a fixed pattern. For example, we note that flat random-noise fields presented stereoscopically cause the image to appear to shimmer, due to an attempt by the visual system to stereoscopically fuse the random bright and dark variations. Thus the question of threshold detection of objects stereoradiographically is different from detection in other stereoscopic settings.

2. MATERIALS AND METHODS

To begin to address the question of radiation dose in stereoscopy we performed an observer study, testing the hypothesis that in combining the left and right eye images by the human visual system, the dose needed for

Further author information: (Send correspondence to A.D.A.M.). P.R.B.: E-mail: pbakic@esther.rad.tju.edu. M.A.: E-mail: albert@esther.rad.tju.edu. A.D.A.M.: E-mail: Andrew.Maidment@mail.tju.edu, Phone: (1 215) 955 5013, Fax: (1 215) 923 1562, Address: Thomas Jefferson University, Department of Radiology, 111 S 11th St., Suite 3390, Philadelphia, PA 19107

Medical Imaging 2002: Physics of Medical Imaging, Larry E. Antonuk, Martin J. Yaffe, Editors,
Proceedings of SPIE Vol. 4682 (2002) © 2002 SPIE ·1605-7422/02/$15.00

each of the two stereoradiographic images is one half of the dose for a single x-ray image viewed monoscopically. Thus, by corollary, we hypothesize that viewing a stereoscopic image will result in an effective increase in SNR by a factor of $\sqrt{2}$.

The observer study consisted of a series of contrast-detail (C-d) experiments with stereoradiographic images acquired over a range of exposures. The C-d experiment belongs to a class of threshold-visibility psychophysical measurements.[8] In the study, observers attempted to detect details in a C-d phantom. The observers scored the phantom both monoscopically (each eye was presented the same radiographic projection) and stereoscopically (each eye was presented a separately acquired radiographic projection). For this experiment we wished to concentrate on the issue of whether the human observer could combine the stereoscopic images in a manner so as to reduce the quantum mottle. Thus, while the two projections in the stereoradiographic pair were acquired separately, they were acquired with the same geometry and no depth information was encoded (i.e., all objects were in the imaging plane, to avoid problems with the variable ability of observers to fuse stereo pairs). Seven observers (six medical physicist and one resident) participated in the study. Stereoscopic visual acuity of the observers was tested separately using the RANDOT test (Stereo Optical Co., Inc., Chicago, IL).

Observer studies of the properties of stereoradiography have been reported in the literature previously. Berkson *et al.*[3] compared the number of false negatives/positives in single (mono) and stereoscopic chest radiographs and Hsu *et al.*[9] studied detection of simulated abnormalities in stereomammography. Kundel *et al.*[6] compared stereoscopic acuity and effects of monocular depth cues under direct vision and in stereofluoroscopy. Goodsitt, Chan, and Hadjiiski[10] studied the depth perception in stereomammography.

2.1. Image acquisition

We imaged an RMI-180 mammographic C-d phantom (Gammex RMI, Middleton, WI). The phantom has 90 objects aligned in nine columns. Objects within the same column decrease in diameter in steps of $\sqrt{2}$, in the range of 7.07-0.312 mm, with constant thickness. The thickness of the objects varies between columns in steps of $\sqrt{2}$, in the range of 1.0-0.062 mm. The images were acquired with a DirectRay flat panel digital x-ray detector (Hologic/Direct Radiography, Newark, DE).[11]

Imaging was performed at 60 kVp and six mAs stations in the range of 2-100 mAs, using a general radiography Bi-150 30/50 x-ray tube (Siemens, Munich, Germany) with tungsten target, measured HVL of 1.34 mm Al (at 60 kVp), and a Heliophos 5S generator (Siemens, Munich, Germany). Additional filtration of 6cm of lucite, positioned near the tube, was used to simulate tissue and appropriately harden the beam. The phantom was imaged in contact with the detector (112 cm from the focal spot) and was placed within a wide lucite frame of equal thickness, providing uniform scatter throughout the whole phantom area. Five images of the phantom were acquired at each mAs station, as well as ten dark field (x-rays off) and ten bright field (x-rays on, with the phantom removed) images. The bright and dark fields were used for correcting the gain and offset variations of the individual detector elements (dels).

2.2. Image processing

The raw acquired phantom images were corrected to compensate for the effects of detector nonuniformity and adjusted for the non-linearity of human contrast sensitivity.

2.2.1. Detector nonuniformity

The dark and bright field correction is a standard procedure for reducing the pixel variations due to the gain and offset variations of dels. Corrected pixel values were computed as:

$$(I_{i,j})_{corr} \;=\; K\,\frac{I_{i,j} - E\{D_{i,j}\}}{E\{B_{i,j}\} - E\{D_{i,j}\}} \;+\; \overline{I}_{new}\;, \tag{1}$$

where I and I_{corr} are the original and corrected pixel values, respectively; $E\{D\}$ and $E\{B\}$ are the averages of the dark and the bright fields, respectively; and, K and $\overline{I}_{new}$ are parameters transforming the range (contrast) and the mean image pixel values. Subscripts i and j denote the position of the pixel in the image array.

Correction was also made for the existence of malfunctioning dels, whose corresponding pixel values are not proportional to the incident x-ray flux and differ significantly from their neighboring pixels. Recently, several researchers have investigated this problem. Aach and Metzler[12] proposed image deconvolution using the spectral analysis of the defect image and Tang *et al.*[13] used wavelet analysis for identification and interpolation of flat panel images used for cone beam CT.

In our case, the average value and the variance of all the dark fields were computed for each del, and the same procedure was repeated for all of the bright fields. First, if the pixels at the same position in the average dark and bright images produced identical values and each had zero variance, that indicated a non-functioning ("dead") del. The pixels corresponding to the dead dels were replaced by the average of their immediate neighbors. Second, we computed the spatial variance within 3x3 pixel neighborhoods of the phantom images. The spatial variance values were then averaged over a small and large neighborhood (of size 3 and 5 pixels in diameter, respectively) and tested against the following criterion:

$$\frac{< \sigma >_{sm}}{< \sigma >_{lg}} > C \, , \tag{2}$$

where $< \sigma >_{sm}$ and $< \sigma >_{lg}$ are the spatial averages of the values of the pixel standard deviations, computed over the small or large neighborhood, respectively, and C is the criterion parameter value. Pixels satisfying the criterion were replaced by the average of their immediate neighbors. We noticed that many of the affected dels were grouped along several vertical and horizontal lines. Selecting the value of parameter C such that all of the pixels along these lines were corrected, a number of pixels randomly distributed over the image were undesirably replaced. Averaging too many pixels might change the statistics of the noise and affect the results of the study. Therefore, we identified the lines of malfunctioning dels in images and directly applied the correction. For the rest of the image, the value of $C = 2.1$, which produced a small number of undesired replacements, was selected.

2.2.2. Non-linear human contrast sensitivity

Human contrast sensitivity is a non-linear function of the luminance. Relative changes in luminance are more easily noticed in bright image areas than in dark areas.[14] "Perceptual linearization" is an image transformation that adjusts the brightness so that equal changes in the quantity being displayed will be equally perceived. The contrast sensitivity of the human visual system is approximated by Barten's model.[15] The model was derived for a standard target of a 2 deg x 2 deg square filled with a horizontal or vertical sinusoidal modulation of 4 cycles/deg, placed in a uniform background of the mean target luminance.[14] The threshold modulation at which the target becomes just visible to the average observer defines the just-noticeable difference, JND, at the luminance value of the background. The interpolation of the luminance levels corresponding to 1023 JNDs is given by the grayscale standard display function:[14]

$$\log_{10} Lum(JND) = \frac{a_0 + a_1 \ln JND + a_2 (\ln JND)^2 + a_3 (\ln JND)^3 + a_4 (\ln JND)^4}{1 + b_1 \ln JND + b_2 (\ln JND)^2 + b_3 (\ln JND)^3 + b_4 (\ln JND)^4 + b_5 (\ln JND)^5} \, , \tag{3}$$

where JND and Lum are the number of just-noticeable differences (i.e., the JND index) and the corresponding luminance value, respectively. Coefficients of the rational polynomial interpolation are given in the DICOM standard.[14]

We have incorporated the grayscale standard display function into the transformation from the flat-panel output 12-bit pixel value to the monitor input 8-bit digital-driver value. This transformation consists of three parts, shown in Figure 1. This decomposition offers flexibility to perform observer studies using different monitors or at different overall brightness or contrast levels.

First, the monitor characteristic, relating luminance levels to the 8-bit digital driver levels, was interpolated from photometric measurements made by a TEK Lumacolor J17 photometer (Tektronix, Beaverton, OR). We measured the luminance values in the center and at the periphery of the monitor and used the average values at 24 digital driver levels for interpolation. A fourth order polynomial fit was used for interpolation with maximum error of 1.68 digital driver levels (0.6%).

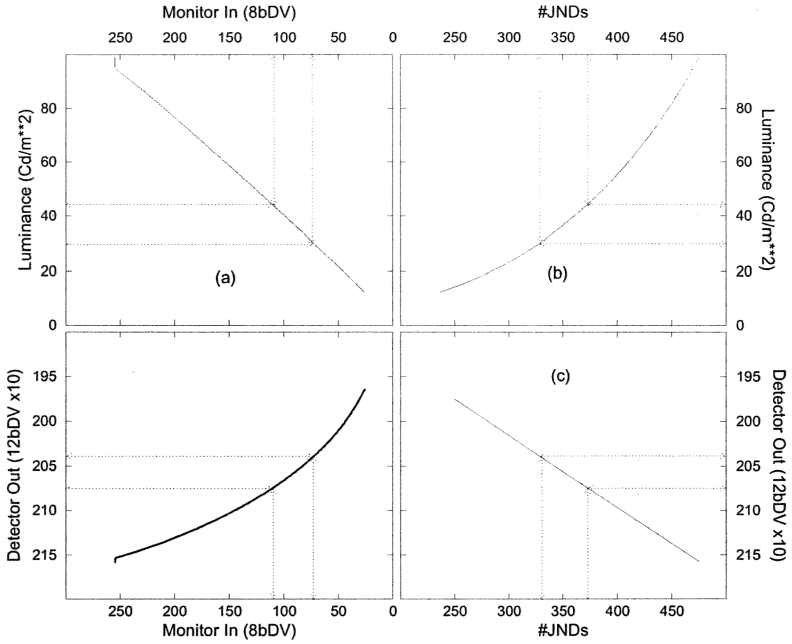

Figure 1. Transformation from the flat-panel detector output to the image on the observer's monitor. (a) Monitor luminance as a function of the driver level, measured with a photometer. (b) Grayscale standard display function, modeling the human contrast sensitivity. (c) Number of JNDs as a function of the flat panel output, used for adjusting the average brightness and contrast of displayed images.

Second, the transformation from the luminance values to the number of JNDs, was approximated by the grayscale standard display function, given by Eq. 3. Third, the linear transformation from 12-bit flat panel output to the JND index was used to adjust the common overall brightness and contrast of all the phantom images used in the study. The overall brightness was selected in a small preliminary observer study as the one which gave the largest increase in number of details seen stereo- vs. monoscopically. Based on that study, the mid-level between the first detail and its annular neighborhood was transformed to a JND index of 350, corresponding to a digital driver level of 90. The range between the average brightness in and around the first detail was mapped to a range of 328-372 JNDs, corresponding to a range of 73-110 digital driver levels. We chose to keep the contrast between the largest phantom detail and its background constant for all the images displayed in the study. (Discussion about this issue is given in Section 3.3.3.) Therefore, the linear transformation from the flat-panel output to the JND index, was image dependent. An example of a processed phantom image is shown in Figure 2.

2.3. Observer study

2.3.1. Selection and display of images

Each observer was presented with 60 images, consisting of 30 for monoscopic viewing and 30 for stereoscopic viewing, 5 images for each of 6 exposure levels. The monoscopic images were displayed so that both the left and right eye saw the same image, while for the stereoscopy, the left and right eye images were different. Each of the observers saw the same set of monoscopic images (since there were 5 images acquired for each mAs). A set of 5 out of twenty possible stereo image pairs for each mAs was selected randomly for each observer.

The two sequences of 30 images, one for mono- and the other for stereoscopic viewing, were randomly permuted separately and then interleaved into a single sequence of the form: ... M_n S_n M_{n+1} S_{n+1} ..., where M_i and S_i represent mono and stereo images, respectively. Next, the positions of the mono and stereo images, in each mono-stereo pair, were randomly changed in order to break the repetition of mono following stereo, and decrease possible observer bias.

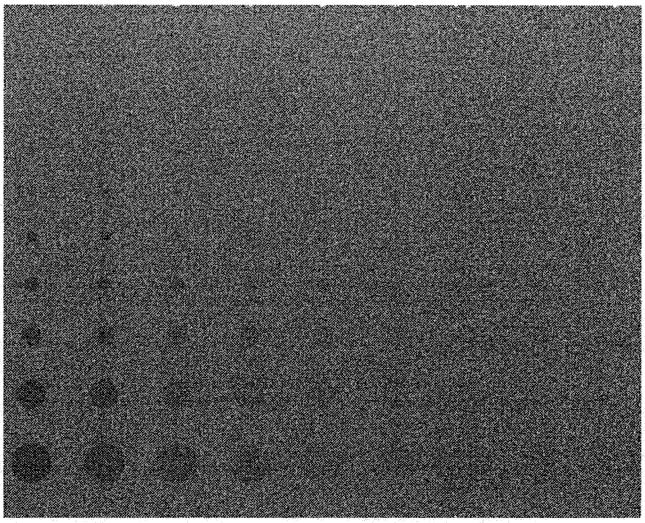

Figure 2. An example of a phantom image used in the study. The image was acquired with an exposure of 10mAs and post-processed to compensate for the effects of detector nonuniformity and to adjust for the non-linearity of human contrast sensitivity.

2.3.2. Viewing conditions and scoring

The experiment was performed in a darkened room, with a black monitor background. The distance between the observer's eyes and the monitor was kept constant at approximately 1 m. Stereoscopic Crystal Eyes goggles (StereoGraphics, San Rafael, CA) were used for both mono- and stereo experiments.

Several training sessions for image scoring were organized for observers in order to establish a uniform decision criterion. The observers were trained to inspect the objects, from larger to smaller size and from larger to smaller contrast. The objects were inspected for general roundness ("whether or not more than 50% of the edge was visible"), size ("whether or not more than 50% of the object was missing"), and the expected position in the detail array. A graphic user interface was developed allowing an observer to assign the smallest detail seen in a column by clicking over the detail position.

2.4. Test of stereoscopic acuity

The stereoscopic acuity of the observers participating in the study was tested using a standard clinical test, the RANDOT Stereotest (Stereo Optical Company, Chicago, IL). The test consists of random-dot image pairs with or without angular disparity.[16] The images in a pair are orthogonally polarized and the stereo effect is observed using appropriately polarized glasses. The images are divided into three groups with different content (geometric figures, animals, and triplets of circles) designed to assess the stereoscopic acuity in a wide range of patients' age. The images in each of the groups gradually decrease in angular disparity and roughly cover the range of 20-500 seconds of arc, when viewed from 40 cm distance. Each image contains one object with angular disparity and the others without. Stereoscopic acuity is measured by identifying the image, and the corresponding angular disparity, for which the observer cannot further distinguish between the objects with and without disparity. Table 1 shows the minimum observable angular disparity for seven observers.

3. RESULTS AND DISCUSSION

The observers took on average 39 minutes (std. dev. = 2.8 minutes) to score a set of 60 combined mono and stereo images. Figure 3 (a) shows the number of details seen mono- and stereoscopically, averaged over all images with the same mAs, for a single observer, and Figure 3 (b) shows the difference between the average number of details for stereo and mono images, for all the observers. We have compared the stereo- and monoscopic performance of the observers by analysis of the C-d curves and an analysis of the SNR.

Table 1. Results of the RANDOT stereo test for seven observers. Tabulated are the values of the minimum observable angle of stereo disparity in seconds of arc.

Observer	$\Delta\alpha_{min}$ [arc sec]
1	25
2	70
3	30
4	200
5	25
6	100
7	25

3.1. C-d curves

We used thickness, t, as a surrogate of the contrast, since for the low contrast objects of interest to this study contrast can be considered proportional to the object thickness. Details were scored by the diameter, d, of the smallest visible object in a column of equal contrast. In an ideal case the detail visibility would be determined only by the SNR$= t\ d\ K\sqrt{\text{mAs}}$, i.e., by the product of the detail thickness and diameter. Thus, the C-d curves would take the form of lines with negative unit slope on a log-log plot, through the points satisfying:

$$\log_{10} t \ + \ \log_{10} d \ = \ \log_{10} \text{SNR}_T \ - \ log_{10} K \ - \ \frac{1}{2} log_{10}(\text{mAs}), \tag{4}$$

where SNR_T is the value of the SNR at the threshold of perception and K is a proportionality constant.

Average C-d curves are computed by averaging the size of the smallest visible detail in each column, over a set of images, e.g., for the same mAs and the same observer. Computing the average detail size is problematic when no details are visible in the same column for one or more images, since the contribution of those images to the average is ambiguous. To avoid this problem, we chose the median diameter for generating C-d curves. Figure 4 (a) shows the average C-d curves for a single observer and Figure 4 (b) shows the C-d curves averaged over six observers. C-d curves in Figures 4 (b) and (d) include the results of all but one of the observers. The observer in question subjectively claimed very low stereoscopic vision, which corresponded to a large value of the minimum observable angular disparity in the RANDOT test results (Table 1, Observer 4), and was also indicated by a significantly smaller difference between the number of details seen stereo- vs. monoscopically (Figure 3 (b), points labeled by triangles).

In order to compare the C-d curves corresponding to stereo- and monoscopic viewing, we have approximated each of the curves by a line with negative unit slope, in agreement with Eq. 4. The difference in the intercept values between the approximated stereo and mono C-d curves can be related to the effective reduction in mAs during stereoradiography (assuming the same threshold SNR for mono and stereo experiments):

$$\log_{10} d_{\text{M}} - \log_{10} d_{\text{S}} \ = \ \log_{10} \frac{d_{\text{M}}}{d_{\text{S}}} \ = \ \log_{10} \sqrt{\frac{(mAs)_{\text{S}eff}}{(mAs)_{\text{M}}}} \tag{5}$$

where d_{M} and d_{S} are the diameters of the smallest visible details viewed mono- and stereoscopically, respectively (for the same detail thickness). $(mAs)_{\text{M}}$ and $(mAs)_{\text{S}eff}$ are the exposure used for acquiring the mono images and the effective exposure of stereoscopic viewing, respectively. $(mAs)_{\text{S}eff}$ is defined as the exposure needed to obtain an image which, when viewed monoscopically, would produce the same C-d characteristic as the stereo image in question. If our hypothesis is true and the dose in stereoradiography is equal to a half of the dose required for monoscopic viewing, then the corresponding linear approximations of the C-d curves would be separated by an intercept of $\sqrt{2}$. Figure 4 (c) shows the linear approximation of the C-d curves for a single viewer (from Figure 4 (a)). Figure 4 (d) shows the linear approximation of the C-d curves for six observers.

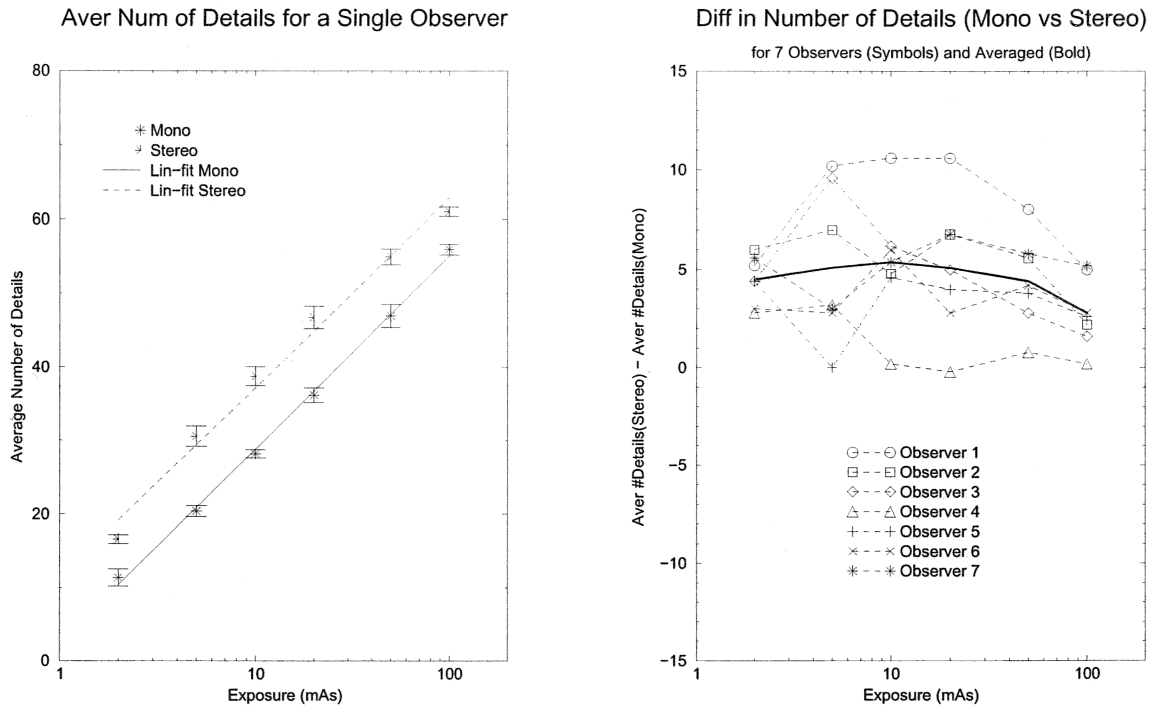

Figure 3. Comparison between the mono- and stereoscopic viewing. (a) Number of seen objects, out of the total of 90 objects, averaged over all 7 observers. (b) Difference in the number of objects seen by stereo- vs. monoscopy, for each observer.

3.2. SNR cut-off

The objects used in this observer study were of low contrast and imaged on a detector with essentially no correlation in the noise between detector elements (a white noise power spectrum). Therefore, for monoscopically viewed images the classic Rose model[17,18] is applicable, in which the signal-to-noise ratio ($\mathrm{SNR}_{\mathrm{mono}}$) can be computed from the subject contrast and the standard deviation in the pixels values, and object visibility is directly related to $\mathrm{SNR}_{\mathrm{mono}}$. The subscript "mono" is used here to emphasize that this is the SNR applicable to an analysis of viewing a single image. In Figure 5 we calculated the number of objects visible as a function of exposure for a class of ideal observers which would detect all objects above a given threshold $\mathrm{SNR}_{\mathrm{mono}}$. Thresholds in $\mathrm{SNR}_{\mathrm{mono}}$ of two through seven are shown; the number of objects decreases with increasing threshold. Superimposed on Figure 5 are the fits to the actual performance of one observer from Figure 3 (b). For monoscopic viewing, the data for this observer falls between the theoretical curves corresponding to $\mathrm{SNR}_{\mathrm{mono}}$ thresholds of 5 and 6, (in agreement with the customary range of estimates of Rose's k). For an observer capable of combining information from stereoscopic (independently acquired) images the signal-to-noise ratio of each object should increase by a factor of $\sqrt{2}$, i.e., ($\mathrm{SNR}_{\mathrm{stereo}} = \sqrt{2}\mathrm{SNR}_{\mathrm{mono}}$), so that the object count as a function of exposure would correspond to a monoscopic signal-to-noise ratio cut-off reduced by a factor of $\sqrt{2}$. Consistent with this, the real observer from Figure 5 does show an increased sensitivity, as will be discussed in detail later.

3.3. Discussion

3.3.1. Performance analysis from the C-d curves

Figure 6 shows a relative reduction in exposure when using stereo- instead of monoscopic viewing, as a function of mAs. Plotted are the percent values of $(d_{\mathrm{M}}/d_{\mathrm{S}})^2 = (mAs)_{\mathrm{S}eff}/(mAs)_{\mathrm{M}}$, normalized with the hypothesized reduction by half (solid curve). (Notation used is the same as in Eq. 5.) The normalization was done so that,

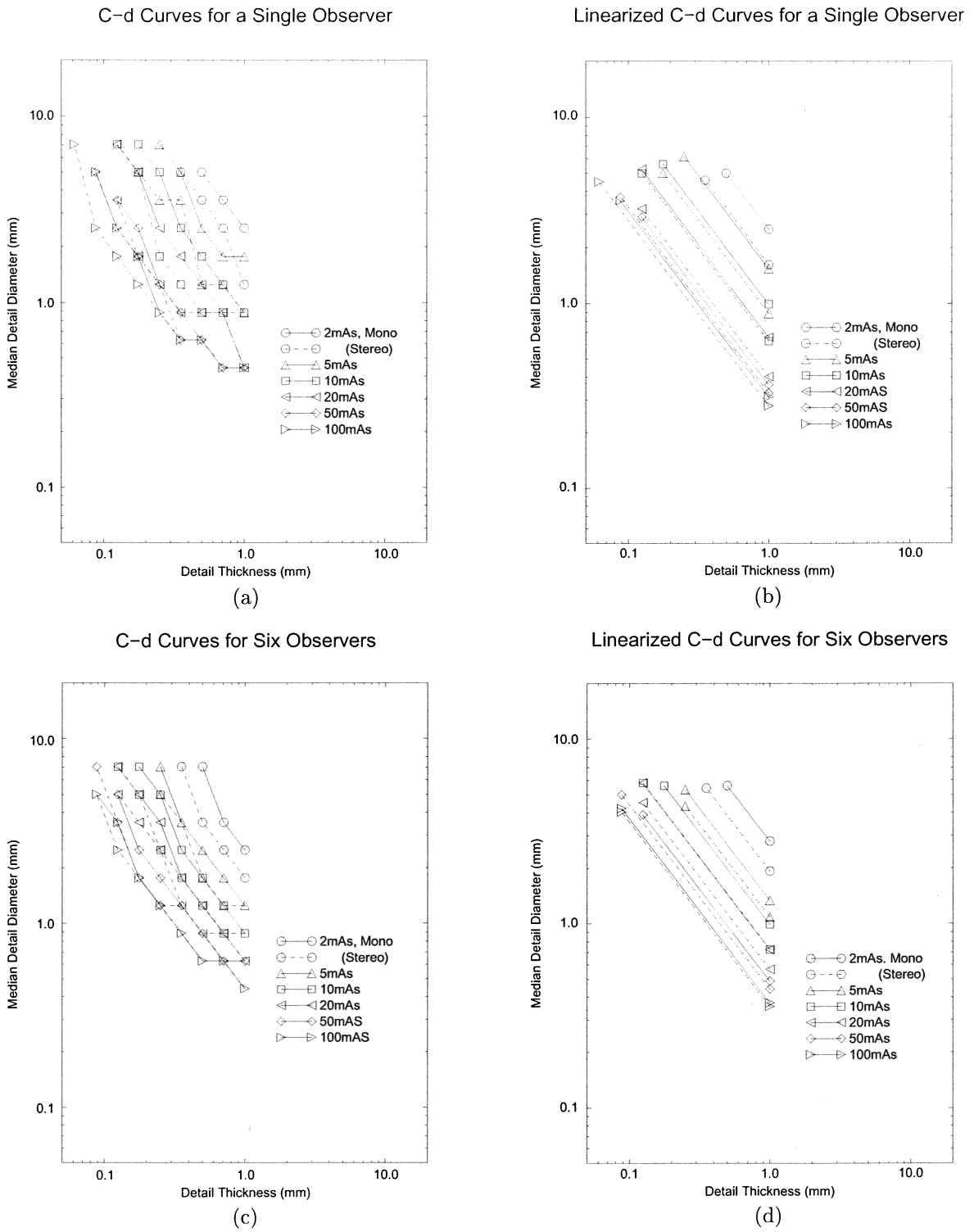

Figure 4. C-d curves for monoscopic (solid) and stereoscopic (dashed) viewing. (a) C-d curves of an observer (#1) averaged over all the images with the same exposure level. (b) Linear approximation of the C-d curves from (a). (c) C-d curves averaged over all the observers, except observer #4 (excluded for very low stereo vision). (d) Linear approximation of the C-d curves from (c).

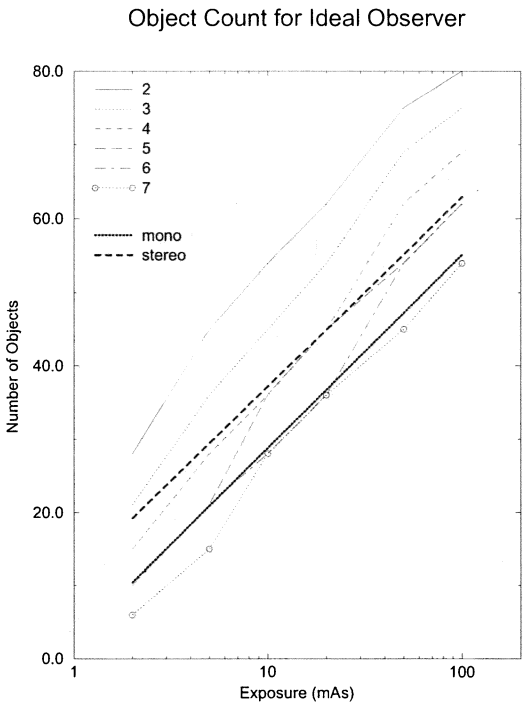

Figure 5. Number of objects visible, out of the total of 90, for an ideal observer (thin lines). The lines are labeled by the corresponding value of the threshold SNR (2-7). Superimposed is the number of objects visible for the real observer from Figure 3 (b) (bold lines).

assuming our hypothesis true, $[(d_{\mathrm{M}}/d_{\mathrm{S}})^2]/2$ would be equal to 100% for all the mAs values. The maximum and minimum values obtained in our study were 113% at 2 mAs and 60% at 100 mAs, respectively.

In addition, the effective stereoscopic exposure relative to the nominal monoscopic exposure of the next higher mAs station, $(d_{\mathrm{M},2\times\mathrm{mAs}}/d_{\mathrm{S,mAs}})^2 = (mAs)_{Seff}/(mAs)_{nextM}$, is plotted on the same graph in Figure 6 (dashed curve). In our study, the nominal exposures increase by a step of 2 for all the mAs stations, except 2mAs and 20mAs (not plotted). Analysis of $(d_{\mathrm{M},2\times\mathrm{mAs}}/d_{\mathrm{S}})^2$ is of interest since it directly compares the observer's performance at the mAs stations whose stereo- and monoscopical results should be equal (100% on the plot) by our hypothesis. We have obtained values in the range of 84-91%.

The solid curve in Figure 6 ("[Stereo vs. Mono]/2") supports our hypothesis that the dose needed for each of the two stereoradiographic images is one half of the dose for a single x-ray image viewed monoscopically, for images acquired at the lower exposures (2-20 mAs). At higher exposures (50-100 mAs), we observed less benefit from stereographic viewing. Potential reasons for this discrepancy are given in Section 3.3.3. The images produced with lower exposures, have quantum noise which was more evident, providing the best simulation of the x-ray quantum noise limited detection.

The other performance measure ("Stereo vs. Next Mono", the dashed curve in Figure 6) shows less variation over the range of exposures used in the experiment. This is also seen in Figure 5 where the measured number of details detected stereoscopically (bold, dashed) approximately equals the number of details detected monoscopically at twice the exposure (bold, dotted). Note that the SNR values (thin, numbered lines in Figure 5), corresponding to the measured number of detected details decrease with increased exposure, which explains in part the decrease of the "[Stereo vs. Mono]/2" performance measure (solid curve in Figure 6) at higher exposures.

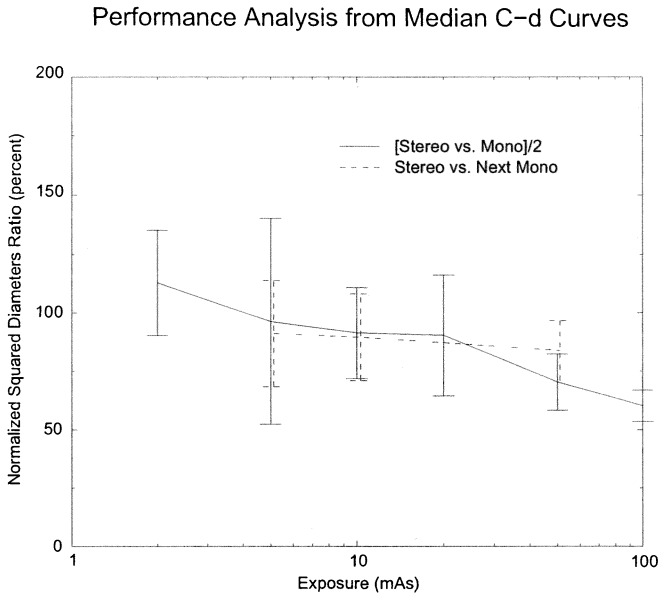

Figure 6. Comparison of the observers mono- and stereoscopic performance using the linearized C-d curves. $[(d_{\mathrm{M}}/d_{\mathrm{S}})^2]/2$ ("[Stereo vs. Mono]/2") as a function of exposure, (*solid curve*). $(d_{\mathrm{M,2\times mAs}}/d_{\mathrm{S,mAs}})^2$ ("Stereo vs. Next Mono") as a function of exposure, (*dashed curve*). Lines show the average values and bars the $\pm 1\sigma$ ranges.

3.3.2. Performance analysis from the SNR cut-off

Following the Rose model, the results were analyzed by identifying a threshold SNR under each viewing condition. For each observer scoring of the phantom, the detected details had greater SNR_T than the details not detected, with only a few details near the threshold not following this pattern. Thus, for each observer scoring of the phantom, the threshold was calculated as the mean of the smallest $\mathrm{SNR}_{\mathrm{mono}}$ of the details detected and the largest $\mathrm{SNR}_{\mathrm{mono}}$ of the details not detected. (Notation used is the same as in Section 3.2.) The averages of these per-scoring values over the 5 monoscopic viewings give the monoscopic threshold $\mathrm{SNR}_{T_{\mathrm{M}}}$ for each viewer at each exposure level, and similarly the 5 stereoscopic viewings give $\mathrm{SNR}_{T_{\mathrm{S}}}$. A hypothetical observer capable of reducing the quantum noise in the phantom images by using information from both images of the stereoscopic pair would then effectively find the signal to noise ratio of each disk increased by a factor of $\sqrt{2}$, and thus would present a decrease in the SNR_{mono} of the threshold objects by a factor of $1/\sqrt{2}$. Thus, for such a hypothetical observer, one expects $\mathrm{SNR}_{T_{\mathrm{M}}}/\mathrm{SNR}_{T_{\mathrm{S}}} = \sqrt{2}$. In Figure 7 the ratio $\mathrm{SNR}_{T_{\mathrm{M}}}/\mathrm{SNR}_{T_{\mathrm{S}}}$ of each observer at each exposure level is plotted, along with the averages over the observers. The ratio is near $\sqrt{2}$ at low exposures, as expected for the hypothetical observer combining information from each of the stereo pair of images. At higher exposures, the ratio is less, but still greater than one.

3.3.3. Further considerations

The following issues are potential sources of concern in our experiment. Since it was, to the best of our knowledge, the first C-d study of the stereo- vs monoscopic viewing in radiography, no reference suggestions were found to address those issues. Future experiments, modified to improve the following conditions, may give a more accurate estimate of the advantages of stereoradiography.

Observers used the stereoscopic goggles while viewing both mono and stereo images, in order to keep the average brightness level comparable and reduce bias of having the stereo images directly identified. The goggles reduce the brightness level of the scene. We have not analyzed the amount of this brightness reduction, nor its uniformity with the change of brightness. Perceptual linearization was applied without taking into account this brightness reduction, and this might be of concern if the non-linearity of the human contrast sensitivity was not

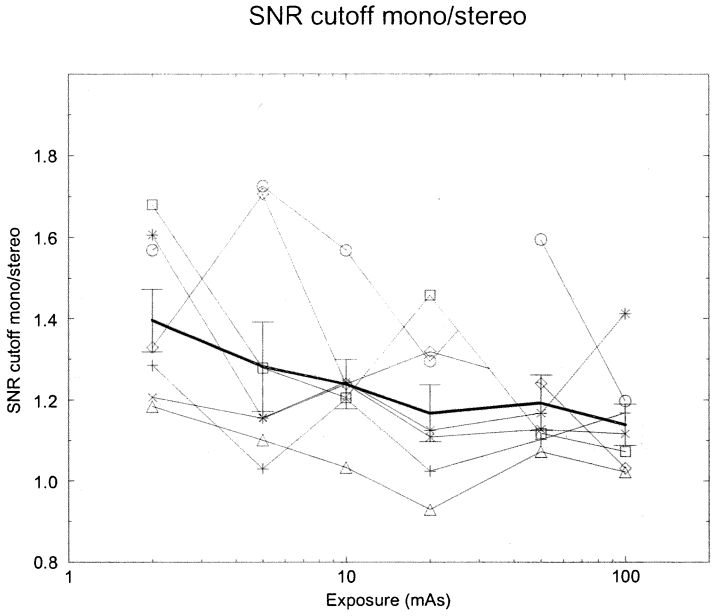

Figure 7. Comparison of the observers mono-and stereoscopic performance using the analysis of the SNR cut-off values. The SNR cut-off values of the individual observers as a function of the exposure, (*solid lines with symbols*). The average SNR cut-off values with the standard deviation ranges, (*bold line*).

properly compensated.

The transformation from the flat panel 12-bit output to the number of JNDs was implemented in an image dependent fashion, keeping the background contrast of the largest detail constant in all of the images displayed to the observer. For the high-contrast images, acquired with high nominal exposure, this caused the background noise range to be limited to only a few 8-bit digital driver levels, with the potential for significant quantization distortion (clipping). The effects of this distortion on the results of the C-d experiment are not obvious. An alternative was to keep constant the standard deviation of the background noise in all displayed images. This will, however, change the contrast of the largest detail in the images with different nominal exposures, which would lead to possible saturation of the display. Note, also, that structured anatomic noise is not included in this set of test images, but its modeling is considered for future research.[19,20] We have also begun another approach to testing the hypothesized benefits of the stereoradiography using a 2-alternative forced-choice experiment.

4. CONCLUSIONS

A series of C-d experiments was performed, testing the hypothesis that the radiation dose required for stereoradiography is one half the dose for a single x-ray image viewed monoscopically, due to the combination of images by the human visual system. For images acquired at a fixed exposure, more objects were detected under stereoscopic than monoscopic viewing conditions. For the lower range of the x-ray exposures tested, where the quantum fluctuations were easily visualized, the increase in the number of details observed was the same as expected for a hypothetical observer combining the two projections to remove noise. With increasing x-ray exposure, the increment between the number of objects detected under stereoscopic and monoscopic conditions decreased, but was always positive. The study results are also influenced by the brightness reduction of stereoscopic goggles, background noise clipping, and the lack of anatomical noise.

ACKNOWLEDGMENTS

The work was funded by the U.S. Department of Defense, Grant DAMD 17-98-1-8169. The authors are grateful to Dan Beideck, Scott Cupp, Natasa Milojkovic, and William Tao Shi for participating in the experiment.

REFERENCES

1. C. A. Jacobi and D. Q. Paris, *Textbook of Radiologic Technology, 6th ed.*, The C.V. Mosby Company, St. Louis, MO, 1977.
2. M. Tortorici, *Concepts in Medical Radiographic Imaging: Circuitry, Exposure, and Quality Control*, W.B. Saunders Co., Philadelphia, PA, 1992.
3. J. Berkson, C. A. Good, D. T. Carr, and A. J. Bruwer, "Identification of "positives" in roentgenographic readings," *Am. Rev. Resp. Dis.* **81**, pp. 660–665, 1960.
4. R. R. Carlton and A. M. Adler, *Principles of Radiographic Imaging: An Art and a Science*, Delmar Publishers, Inc., Albany, NY, 1992.
5. R. W. Reading, *Binocular Vision: Foundations and Applications*, Butterworths, Boston, MA, 1983.
6. H. L. Kundel, P. R. Lynch, L. Peoples, and H. M. Stauffer, "Evaluation of observer performance using televised stereofluoroscopy," *Investigative Radiology* **2**, pp. 200–207, 1967.
7. F. W. Campbell and D. G. Green, "Monocular versus binocular visual acuity," *Nature* **208**, pp. 191–192, 1965.
8. G. Cohen, "Contrast-detail analysis of imaging systems: Caveats and kudos," in *Recent Developments in Digital Imaging*, K. Doi, L. Lanzl, and P.-J. P. Lin, eds., pp. 141–159, American Institute of Physics, New York, 1985.
9. J. Hsu, D. M. Chalberg, C. F. Babbs, Z. Pizlo, and E. Delp, "Preclinical roc studies of digital stereomammography," *IEEE Trans. Med. Imaging* **14**, pp. 318–327, 1995.
10. M. M. Goodsitt, H.-P. Chan, and L. Hadjiiski, "Stereomammography: Evaluation of depth perception using a virtual 3D cursor," *Med. Phys.* **27**, pp. 1305–1310, 2000.
11. E. L. Gingold, D. L. Y. Lee, L. S. Jeromin, B. Rodricks, M. G. Hoffberg, and C. L. Williams, "Development of a novel high-resolution direct conversion x-ray detector," in *Medical Imaging: Physics of Medical Imaging*, J. T. D. III and J. M. Boone, eds., *Proc. SPIE* **3977**, pp. 185–193, 2000.
12. T. Aach and V. Metzler, "Defect interpolation in digital radiography – how object-oriented transform coding helps," in *Medical Imaging: Image Processing*, M. Sonka and K. M. Hanson, eds., *Proc. SPIE* **4322**, pp. 824–835, 2001.
13. X. Tang, R. Ning, R. Yu, and D. Conover, "Cone beam volume ct image artifacts caused by defective cells in x-ray flat panel imagers and the artifact removal using a wavelet-analysis-based algorithm," *Med. Phys.* **28**, pp. 812–825, 2001.
14. *DICOM Standard PS-3.14-2000: Gray-scale Standard Display Function*, National Electrical Manufacturers Association, Rosslyn, VA, 2000.
15. P. G. Barten, "Physical model for the contrast sensitivity of the human eye," in *Human Vision, Visual Processing and Digital Display*, B. E. Rogowitz, ed., *Proc. SPIE* **1666**, pp. 343–348, 1992.
16. B. Julesz, *Foundations of Cyclopean Perception*, The University of Chicago Press, Chicago, IL, 1971.
17. A. Rose, *Vision: Human and Electronic*, Plenum, New York, NY, 1973.
18. A. E. Burgess, "The Rose model, revisited," *J. Opt. Soc. Am. A* **16**, pp. 633–646, 1999.
19. F. O. Bochud, C. K. Abbey, and M. P. Eckstein, "Statistical texture synthesis of mammographic images with clustered lumpy backgrounds," *Optics Express* **4**, pp. 33–43, 1999.
20. P. R. Bakic, M. Albert, A. D. A. Maidment, and D. Brzakovic, "Mammogram synthesis using a 3-d simulation," *submitted to Medical Physics* .